Hindawi
Journal of Chemistry
Volume 2022, Article ID 9647793, 11 pages
https://doi.org/10.1155/2022/9647793

Research Article

Pomegranate Peel Extract-Mediated Green Synthesis of ZnO-NPs: Extract Concentration-Dependent Structure, Optical, and Antibacterial Activity

Adnan Alnehia,[1,2] **Abdel-Basit Al-Odayni**,[3,4] **Annas Al-Sharabi**,[2] **A. H. Al-Hammadi**,[1] **and Waseem Sharaf Saeed**[3]

[1]*Department of Physics, Faculty of Sciences, Sana'a University, Sana'a 12081, Yemen*
[2]*Department of Physics, Faculty of Applied Sciences, Thamar University, Dhamar 87246, Yemen*
[3]*Engineer Abdullah Bugshan Research Chair for Dental and Oral Rehabilitation, College of Dentistry, King Saud University, Riyadh 11545, Saudi Arabia*
[4]*Department of Chemistry, Faculty of Education, Thamar University, Dhamar 87246, Yemen*

Correspondence should be addressed to Adnan Alnehia; adnanalnahia83@gmail.com and Abdel-Basit Al-Odayni; aalodayni@ksu.edu.sa

Received 17 August 2022; Revised 15 September 2022; Accepted 23 September 2022; Published 6 October 2022

Academic Editor: Mahmood Ahmed

Plant-based nanoparticles (NPs) have many advantages over physical and chemical methods and featured with several medicinal and biological applications. In this study, zinc oxide NPs (ZnO-NPs) were synthesized using *pomegranate peel* aqueous extract, under mild and ecofriendly conditions. The ZnO-NPs structure, morphology, and optical properties were investigated using X-ray diffraction (XRD), scanning electron microscope (SEM), Fourier transform infrared (FTIR), and ultraviolet-visible (UV-Vis). Antibacterial activity against Gram-positive and Gram-negative strains were evaluated using the disk diffusion method. The effect of extract concentration (20, 30, and 40 mL) on the final properties of NPs, as well as the NPs concentration used for antibacterial test (50, 100, and 200 mg/mL), were also studied. The results indicate a hexagonal structure with particle size increases as extract concentration increase (D = 18.53, 29.88, and 30.34 nm), while the optical bandgap was decreased (E_g = 2.87, 2.80, and 1.92 eV). The antibacterial activity of ZnO-NPs indicated high efficiency, similar or even higher than that of the control azithromycin, more against *S. aureus*, increased with NPs concentration, and preferred when NPs prepared from high extract concentration. Such promising physicochemical properties support the usefulness and efficacy of the reported bio-route for production of ZnO-NPs and may encourage its application for large-scale production.

1. Introduction

Plant-mediated synthesis of NPs is an innovative industrial technique with plenty of profitable and ecofriendly features [1, 2]. Green synthesis of metal and metal-oxide NPs is one interesting issue of nanoscience, with plants seem to be the best candidates for the large-scale application [3]. The use of plant extract for making such NPs is, on the one hand, cost-effective, easy to be scaled up, and environmentally benign and, on the other hand, the resulting nanoproduct is more stable and tailored in shapes and sizes compared to those obtained by other organisms [3, 4].

Among metal oxide NPs, ZnO nanostructures are the forefront of research due to their unique features and wide applications. ZnO-NPs can be synthesized through several ways such as chemical (sol-gen and solvothermal), physical (evaporation-condensation and laser ablation), and biological methods. Due to the use of organic solvents and the nature of chemical reactions that may produce harmful chemicals for environment and human being which possibly adsorbed on the NPs' surface, the chemical method is not

favored in production of NPs. Likewise, physical methods are associated with some difficulties like the high cost and requirement of harsh conditions such as high pressure and temperature [5, 6]. Thus, biosynthesis has increasingly become a focus of research interest in this field, providing attractive alternative to the conventional chemical and physical methods, due to its simplicity, eco-friendliness, low price, and considerable antimicrobial activity [3, 7]. Besides of its simplicity, biosynthesis commonly needs no expensive equipment or training, while it provides pure products.

It is known that the nature of biological entities (extract, enzymes, and proteins) used to reduce, and stabilizeation of NPs influence their end-properties, of the synthesized NPs including their structure, shape, size, and morphology, and thus, bioactivity. Using plants as biogenic source for biosynthesis of NPs, the plant type, extraction protocol, solvent employed, and extract concentration play an important role in the properties of the NPs, with precursor concentration being the significant factor affecting the morphology of the synthesized ZnO-NPs. Besides bacteria strain, the bioactivity has been reported to also depend on concentration and morphology of ZnO-NPs [8].

ZnO-NPs prepared using plant extracts have shown favored optical and biological properties compared with those from conventional methods of synthesis [3, 5, 9–11]. In addition, biosynthesis of such metal-oxide NPs is one advantageous method, due to the wide concern of pollution, principally because the concept of environmental protection is now deeply rooted in the expectations of the population [8, 12].

Pomegranate is a familiar, sweet tasting fruit with hard pericarps. A fruit yields about half of its weight in juice, which leads to a lot of peel waste [13, 14]. The peel contains a variety of biologically active compounds those evidently responsible for their reported higher antibacterial properties [13–17] than leaves and flowers.

At this point, *pomegranate peel* was targeted for synthesis of ZnO-NPs through a fabricated route. The obtained ZnO-NPs was fully characterized for its structural and optical properties using FTIR, XRD, SEM, and UV-Vis techniques. Then, the bioactivity against selected bacteria strains was evaluated in reference to azithromycin as a standard drug using the diffusion method.

2. Materials and Methods

2.1. Materials. All chemicals, including zinc nitrate hexahydrate ($Zn(NO_3)_2{\cdot}6H_2O$; ≥99%), sodium hydroxide (NaOH; 98%), and ethanol (EtOH; 99.5) were purchased from BDH Chemical Ltd. (Pool, England, UK) and used as received without further purification. Distilled water (DW) was used wherever required.

2.2. Pomegranate Peel Collection. The *peels of the pomegranate* fruit (PP) were collected from a local market at Thamar city (Thamar, Yemen) during the second half of summer season, 2021. The fruit originally comes from Saadah farms, Saadah governorate, Yemen, and freshly sales within two-to-three weeks of harvesting. To remove the dust particles, the peels were washed thoroughly four-to-five times with tap water, then by DW three times. The clean peels were left to dry at room temperature for three weeks. After that, the dried peels were ground to fine powder with the help of electrical grinder.

2.3. Preparation of Aqueous Extract. Typically, 15 g of PP dry powder were mixed with 200 mL DW to prepare the extract (termed PPE). The mixture was stirred at room temperature ($24 \pm 2^{\circ}C$) for 30 min during which the color of the media was changed from colorless to yellow. Subsequently, the solution temperature was increased and left at boiling for 5 min, then cooled to room temperature, filtered with Whatman No. 2 filter paper and used freshly as obtained for the synthesis of the target ZnO-NPs.

2.4. Biosynthesis of ZnO-NPs. To 25 mL aqueous solution of $Zn(NO_3)_2{\cdot}6H_2O$ (5 g, 0.67 M), 10 mL of NaOH aqueous solution (1.5 g, 3.75 M) was added slowly over about 5 min, followed by dropwise addition of 20 mL of freshly prepared PPE. Upon completion of addition, the mixture was stirred at room temperature for 90 min, then filtered. The obtained precipitate was thoroughly and sequentially washed with ethanol and DW and left to dry at room temperature for 48 h. After that, the dry powder was annealed at 200°C for 3 h to obtain ZnO (termed Z20). The same protocol was applied to prepare Z30 and Z40 in which the volumes of the extract used (i.e., PPE) were 30 and 40 mL, respectively. The overall scheme for biosynthesis of ZnO-NPs and its bioactivity are summarized in Figure 1.

2.5. Biological Studies

2.5.1. Antibacterial Test. The *in vitro* antibacterial activity of the synthesized ZnO-NPs (Z20, Z30, and Z40) was evaluated by screening against Gram-positive (*Staphylococcus aureus* (*S. aureus*)) and Gram-negative (*Escherichia coli* (*E.coli*)) bacteria using the disk-diffusion method as described in the literature [18] and in reference to Azithromycin (AzM) standard drug. The test bacteria were kind gifts from Al-Jarfi medical Lab (Thamar city, Yemen). The media, nutrient agar (Himedia, Mumbai, India) was prepared in accordance with the manufacturer's recommendation. Hence, freshly bacteria suspension was made to an inoculum density equivalent to 0.05 McFarland (1.5×10^8 CFU (colony-forming unit)/mL)). The agar plates were inoculated with the test bacteria with the aid of sterilized swabs. The ZnO-NPs were suspended by sonication in DW to obtain 50, 100, and 200 mg/mL concentrations and used for antibacterial tests [5]. Sterile filter paper disks with diameters of 6 mm were fabricated and immersed in the NPs suspensions. Similarly, disks of AzM and DW were also prepared and used as positive and negative controls, respectively. The paper disks were placed aseptically on the surface of bacterially seeded Petri dishes and incubated at 37°C for 21–22 h. The zone of inhibition (ZOI)

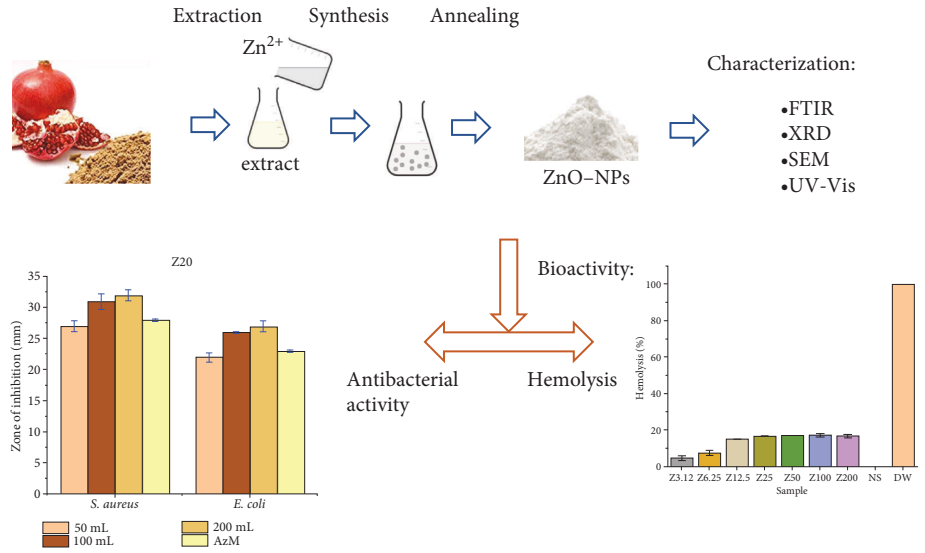

Figure 1: biosynthesis route of ZnO-NPs using *pomegranate peel* extract, characterization methods, and bioactivity.

was determined by measuring the diameter of the inhibition area in mm [19, 20].

2.5.2. Hemolytic Assay. The biosafe nature of the synthesized biogenic ZnO-NPs was assessed using the hemolytic assay against human red blood cells (RBC), following a method described elsewhere [21] with slight modification. Briefly, fresh blood was collected from healthy individuals with a sterile needle (a 25-year-old male volunteer with an O-positive-blood group) after the provision of informed consent. The blood was then dispersed in EDTA-containing tubes to prevent clotting, and RBCs were isolated by centrifugation (1 mL blood) at 4000 rpm for 10 min, followed by careful removal of supernatant and washing the pellet with normal saline solution (NS; 0.9 w/v% sodium chloride, pH 4.5–7.0; Pharmaceutical Solutions Industry, Jeddah, Saudi Arabia). Erythrocyte suspension was then prepared in NS to obtain 2% cell suspension. Test samples of ZnO-NPs were prepared in NS to final concentrations of 3.12–200 μg/mL. To previously marked test tubes containing 0.5 mL of the cell's suspension, 0.5 mL of each test samples, NS (negative control), and DW (positive control) were added, immediately transferred into 37°C incubator, and left for 60 min. After incubation, the solutions were centrifuged at 4000 rpm for 10 min and the separated supernatant was photometrically measured for the released free hemoglobin at 540 nm.

The hemolytic activity was calculated using the following formula (Equation (1)):

$$\%\ \text{hemolysis} = \left(\frac{A_S - A_N}{A_P - A_N}\right) \times 100, \quad (1)$$

where A_S, A_N, and A_P are the absorbance of the test sample (ZnO-NPs), negative control (NS), and positive control (DW), respectively.

2.6. Characterization. The diffraction patterns of ZnO-NPs were obtained using an XD-2 X-ray diffractometer (Beijing Purkinje General Instrument Co., Ltd., Beijing, China), with $CuK_{\alpha 1}$ radiation of $\lambda = 1.54$ Å, in the 2θ range of 10 to 80 and scanning rate of 0.02 min^{-1}. The electronic spectra were recorded on a U-3900 UV-Vis spectrophotometer (Hitachi, Tokyo, Japan), over wavelength range of 200–900 nm at room temperature. Electron micrographs were obtained for NP sputter coated with gold samples, using a JSM-6360 LV SEM (Jeol Ltd., Tokyo, Japan). FTIR spectra were measured on a Nicolet iS10 FTIR spectrometer from Thermo Scientific (Madison, WI, USA), equipped with an attenuated total reflection (ATR, diamond crystal) accessory, over the range of 650–4000 cm^{-1}, with 32 scans per spectrum and 4 cm^{-1} scanning resolution at room temperature.

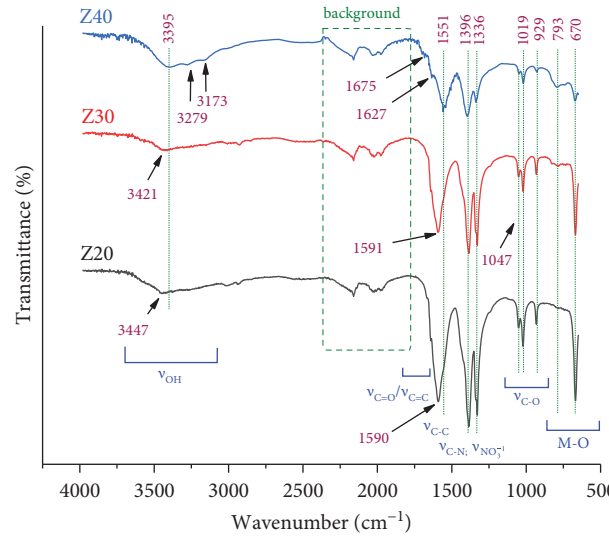

Figure 2: FTIR pattern of the synthesized PPE-mediated ZnO-NPs.

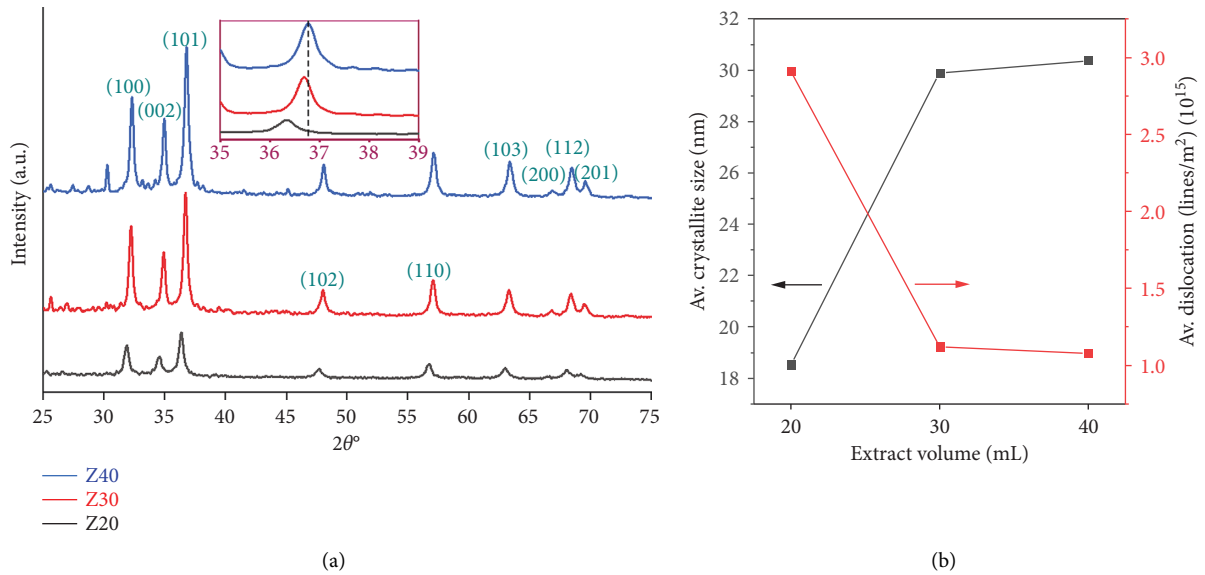

FIGURE 3: (a) X-ray diffraction (XRD) pattern of the synthesized ZnO NPs (Z20, Z30, and Z40); inset is a magnification of the prominent peak of (101) plane. (b) Crystallite sizes (D, nm) and dislocation (δ) vs. extract volume (20–40 mL).

3. Results

3.1. Structural Characterization

3.1.1. FTIR Analysis. Figure 2 represents the FTIR spectra of the PPE-mediated ZnO-NPs (Z20, Z30, and Z40). The spectra are accompanied with indicative peaks of the obtained NPs and traced capping agents from pomegranate peels. The broadband on the range 3070–3550 cm^{-1}, in which at least three peaks were identifiable at 3396, 3278, and 3169 cm^{-1} and more clearly in the spectrum of the Z40 sample was attributed to various v (OH) and v (NH_n) groups, including Zn-OH, free and H-bonding water-OH [22, 23], alcohols, and amides that possibly are a part of NPs-stabilizing compounds, and the capping agents. The peaks at 1675 and 1627 cm^{-1} assigned to $C=O$ and $C=C$ stretching bands of flavonoids and amides in the extract [24] are weak, suggesting their contribution in ZnO-NPs stabilization. These bands were highly overlapped with C-C absorbance around 1590 cm^{-1} and being almost invisible in the spectra of Z20 and Z30, possibly due to their sourced low contents. Absorption at 1590, 1591, and 1551 cm^{-1} in Z20, Z30, and Z40, respectively, is associated with C-C stretching band and its high intensity may indicate its abundance due to reduction of alkenes involved in the production of ZnO-NPs [24, 25]. Besides, the bands at 1396 and 1336 cm^{-1} may characterize C-N stretching or CH and OH bending vibrations of aromatic structures. Hence, it is reported that the amide group, amino, carbonyl group, and polyphenolic compounds in the PPE are a part of redox reaction, dispersion, capping, and stabilizers involved in the production of nanoparticles during the process of synthesis [24, 26, 27]. Bands at 1019 and 929 cm^{-1} are ascribed to asymmetric and symmetric stretching vibrations of C-O-O bonds [27].

The characteristic peaks of ZnO-NPs usually seen on the fingerprint frequencies, i.e., below 900 cm^{-1}. However, due to capacity limit of the ATR-FTIR instrument (4000–650 cm^{-1}), peaks below 650 cm^{-1} were, unfortunately, not reported. Nevertheless, the spectra are incorporated with strong peaks at 670 cm^{-1} which proposed the formation of ZnO-NPs [1].

3.1.2. XRD Analysis. The XRD patterns of the synthesized PPE-mediated ZnO-NPs are shown in Figure 3(a). The spectra exhibit nine diffraction peaks on the range of $2\theta^{\circ}$ 25–75 and some of these peaks are detailed in Table 1. The diffractograms have ascertained material purity with no other external peaks observed, suggesting that the applied method of synthesis is effective to obtain ZnO-NPs of high purity. However, unidentifiable peak at $2\theta^{\circ}$ of 30.10 in Z20 profile may be due to some organics in the extract. Furthermore, the analysis revealed a hexagonal phase as compared with the database (JCPDS No. 36–1451). It is obvious that the diffraction peaks are moderately broad and, thus, indicating highly crystalline ZnO-NPs. According to the literature [28, 29], the broad peak is an indication of small and fine NPs (nanoscale crystalline particles) while the narrow or low intensity peak signifies low crystallinity of the NPs. As shown in Figure 3(b) and Table 1, the average particle diameter (D) of the biosynthesized ZnO-NPs, which calculated using the Debye–Scherrer equation (Equation (2), were between 18.53 and 30.38 nm [30–32]. The dislocation density (δ) of the fabricated samples is specified using the Williamson and Smallman's relation (Equation (3)) [33, 34].

$$D = \frac{k\lambda}{\beta \cos\theta}, \tag{2}$$

$$\delta = \frac{1}{D^2}, \tag{3}$$

where D is the crystallite size, k is a constant denotes the shape factor (0.94), λ is the diffraction wavelength of CuKα

Table 1: Structural parameters of ZnO-NPs.

Samples	2-Theta	*d*-spacing	FWHM (deg)	Planes (hkl)	Crystallite sizes (D, nm)	Average (*D*, nm)	Average dislocation (lines/m^2) (10^{15})
Z20	31.801	2.811	0.566	100	14.59	18.534	2.91
	34.539	2.594	0.381	002	21.83		
	36.339	2.470	0.475	101	17.60		
	47.423	1.915	0.703	102	12.34		
	56.700	1.622	0.343	110	26.31		
Z30	32.141	2.854	0.344	100	24.03	29.878	1.12
	34.321	2.610	0.157	002	52.96		
	36.680	2.448	0.340	101	24.62		
	47.979	1.894	0.405	102	21.47		
	57.039	1.613	0.426	110	21.22		
Z40	32.279	2.771	0.340	100	24.33	30.378	1.08
	34.939	2.565	0.294	002	28.32		
	36.780	2.441	0.390	101	21.46		
	47.535	1.911	0.139	102	62.45		
	57.081	1.612	0.590	110	15.33		

Table 2: Geometric parameters of ZnO-NPs as computed from XRD.

Samples	Lattice parameters (Å)			(*c*/*a*) ratio	Volumes of unit cell (Å^3)	Volumes of particles, V (nm)^3	Atomic packing factor (%)	Degrees of crystal lattice distortion (R)
	a	b	c					
Z20	3.246	3.246	5.199	1.602	47.44	3331.85	75.4582	1.019559
Z30	3.265	3.265	5.204	1.600	48.04	13958.3	75.82696	1.024541
Z40	3.216	3.216	5.222	1.620	46.77	14670.9	74.43153	1.005687

($\lambda = 1.5406$ Å), β is the full width at half maximum (FWHM), θ is the diffraction angle, and δ is the dislocation density. Figure 3(a) (insert) represents the shifting in the peak position toward higher angle with crystallite size increase which, in turn, reflect the effect of preparation extract volume [35]. Other structural parameters such as *d*-spacing (Å), *a* (Å), *c* (Å), *c*/*a* ratio, unit cell volume v (Å)^3, the volume of particles *V* (nm)^3, atomic packing factor (%), and the degree of crystal lattice distortion (*R*) were also computed [36, 37], and the corresponding values are gathered in Table 2.

3.1.3. SEM Analysis. Figure 4 shows the SEM micrograph of the synthesized ZnO-NPs (Z20, Z30, and Z40) in which the ZnO were mainly composed of nanoplatelets with an overall quite dense morphology. The nanosheets' thickness could be estimated to a tenth of nm; however, the thicker sheets may consist of several sheets aggregated to form the nanoplate network [27], with irregular NPs having almost spherical shapes [5]. Such aggregation and flaky agglomeration could be due to a high surface energy of the NPs and also perhaps due to densification of the narrow space between NPs [38]. A similar morphology of ZnO-NPs was also reported by a number of researchers [11, 39]. It seems that the aggregation, as well as the flake thicknesses, become less for ZnO-NPs produced at lower extract concentrations and this may explain the decreased bioactivity on the same order, i.e., antibacterial activity order Z20 > Z30 > Z40.

3.1.4. UV-Vis Analysis. Figure 5 shows the UV-Vis spectra of the ZnO-NPs prepared with various PPE concentrations (Z20, Z30, and Z3). The spectra revealed characteristic maximum absorbances at 370, 375, and 378 nm, respectively, indicating quantum size effects [38]. The bandgap energy (E_g) as calculated from Tauc's plotting for the direct allowed transition, described by Equation (3) [40–42], was found at 2.87, 2.80, and 1.92 eV, respectively for ZnO-NPs (Z20, Z30, and Z40) prepared using different extract volumes (20, 30, and 40 mL) (Figures 5(b)–5(d))).This denotes that the extract volume has an impact on the resulting bandgap of the synthesized ZnO-NPs, i.e., with PPE extract volume increase, the E_g decreased.

$$\alpha h\nu = C\,(h\nu - Eg)^n. \tag{4}$$

Typically, the E_g depends on the structure, size, and shape of the nanoparticles and, therefore, the employment of different extract volume can adjust such properties. By increasing PPE volume, a red shift in the optical bandgap is observed. Such an effect is obviously the result of the organic compounds amount differences present in the extract. According to the literature [13], the PPE is rich with phenolic compounds that may drive production of the ZnO-NPs which further affected by the extract volume used, i.e., the magnitude of phytocompounds.

3.2. Antibacterial Activity of ZnO-NPs. The antibacterial activity of the biosynthesized ZnO-NPs was tested against

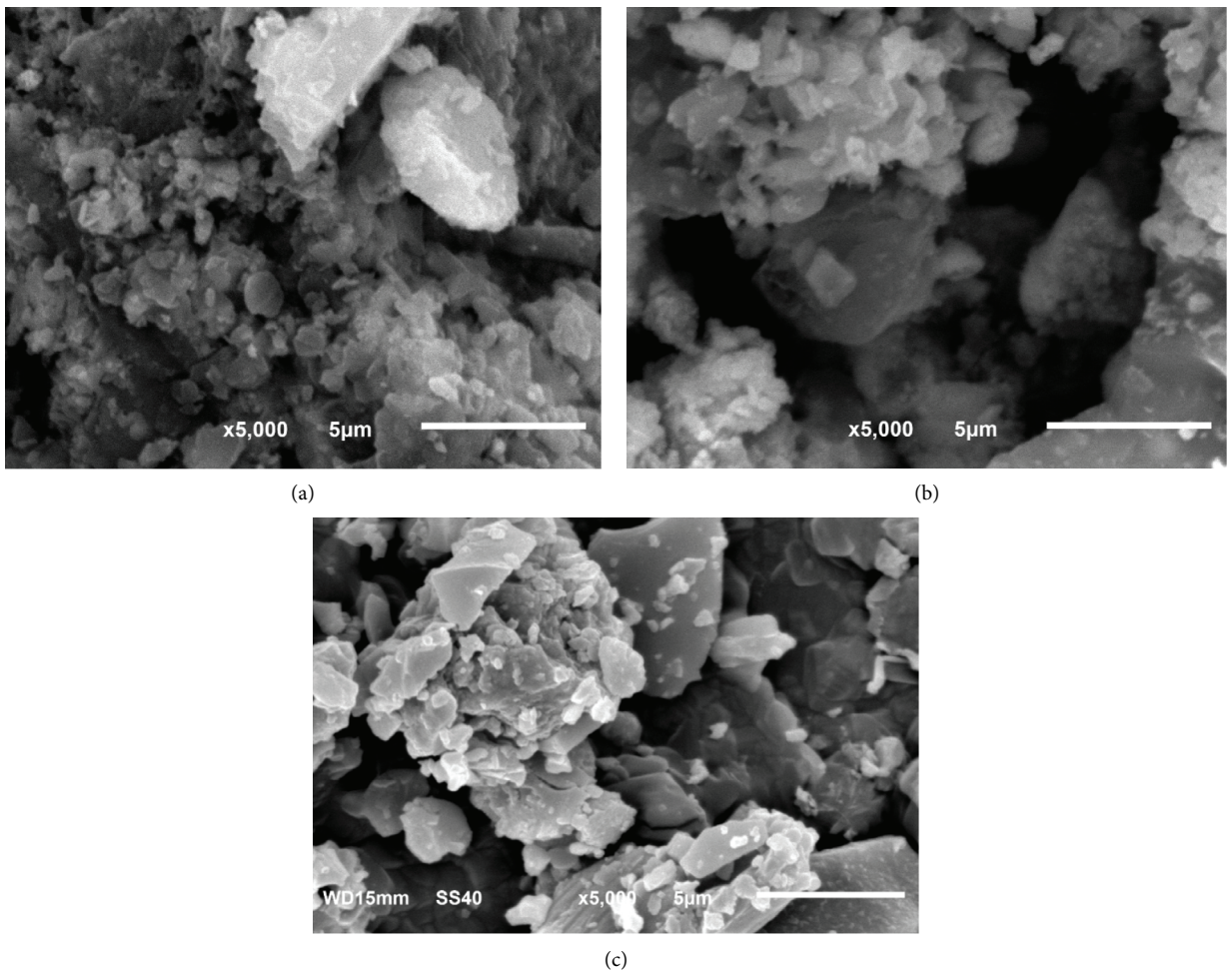

Figure 4: Scanning electron microscope (SEM) image of ZnO-NPs. (a) Z20; (b) Z30; (c) Z40.

both Gram-positive (*S. aureus*) and Gram-negative (*E. coli*) bacteria using the disk-diffusion method. For this, three different concentrations 50, 100, and 200 mg/mL of the biosynthesized ZnO-NPs (Z20, Z30, and Z40) were prepared and used for antibacterial activity studies in comparison to AzM as a standard drug. The resulting zones of inhibition (ZOI) are summarized in Table 3, and selected images of inhibition plates are given in Figure 6. It was observed that all the tested ZnO-NPs have an inhibitory effect against *S. aureus* and *E. coli* similar to or higher than the AzM standard drug. The ZOI was higher against the Gram-positive bacteria (*S. aureus*) compared to Gram-negative bacteria (*E. coli*). This might be due to the fact that Gram-positive bacteria are less susceptible to antibacterial potency than Gram-negative bacteria, perhaps this is a result of their different cell wall structures [43].

In the Gram-positive strain, peptidoglycan is thick while being thinner in the Gram-negative strain, but contains an outer membrane consisting of lipopolysaccharides that provides the bacteria resistance to prepared ZnO and makes them less susceptible [44]. The antibacterial potency of ZnO-NPs against microorganisms depends on cell wall integrity [43, 45]. The results indicate that the use of *pomegranate peel* extract-mediated synthesis of ZnO nanoparticles can be more efficient against Gram-positive bacteria and Gram-negative bacteria. This may be due to the existence of the higher number of phenolic compounds. Moreover, the results illustrated that the prepared samples have a strong antibacterial activity against both the strains compared to Azithromycin.

It is obvious that the ZOI is low for ZnO-NPs prepared using Z40, the case that can be attributed to the higher particle sizes of Z40 (30.34 nm) compared to those of Z20 (18.53 nm) and Z30 (29.88 nm). The highest antibacterial activity for the lower particle sizes, e.g., Z20, is due to their smaller size (18.53 nm) which, in turn, means increased active surface area that further facilitates ease interaction with the bacterial wall [40]. With the increase in ZnO-NPs concentration from 50 to 200 mg/mL, a gradual increase in the bacterial inhibition was also observed, supporting the concentration-dependence activity of the NPs [46, 47].

The bioactivity of NPs could be attributed to various factors such as chemical composition, particle size and shape, concentration, surface charge, and exposure time. The destructive action of ZnO-NPs on microorganisms could be due to one or simultaneous mechanisms: (i) attachment of NPs to a bacterial surface [46], hence the following stepwise events were proposed to be involved in adsorption of NPs on

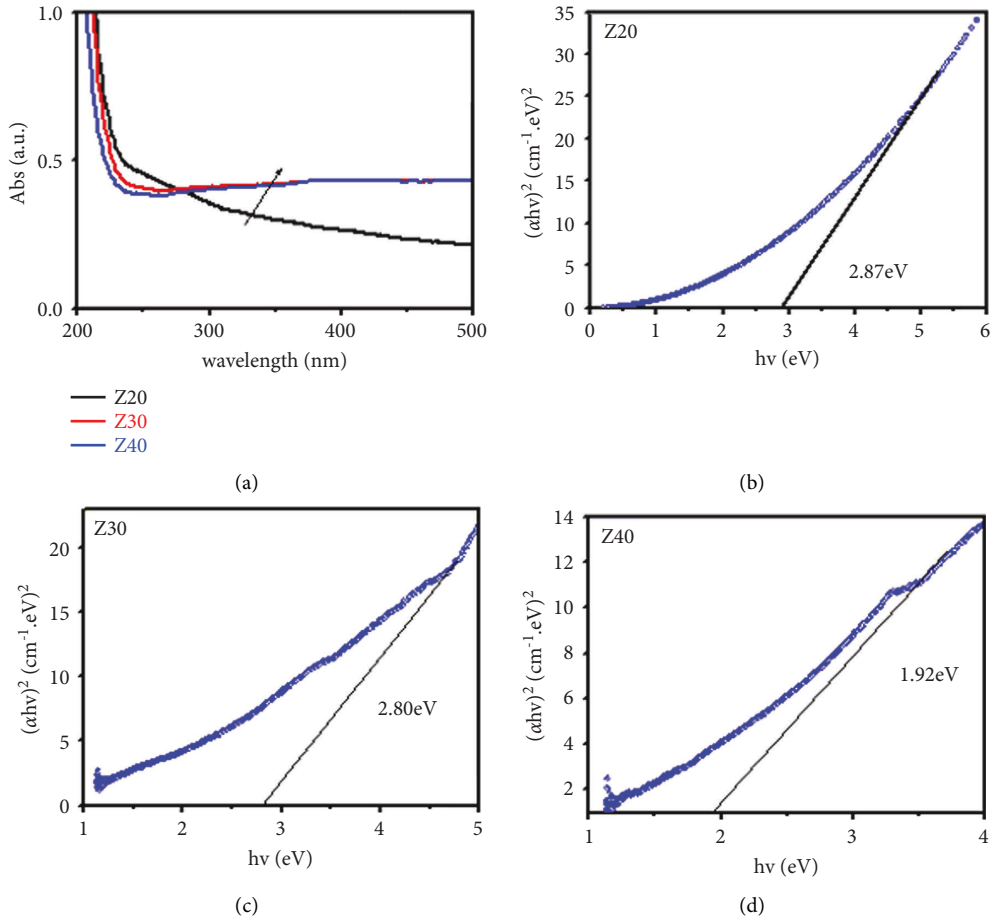

Figure 5: Absorption spectra of ZnO nanoparticles (a) and determination of E_g (b, c, and d).

Table 3: Antibacterial activity of ZnO-NPs using the zone of inhibition method compared to Azithromycin standard drug.

Samples	Bacteria	Zone of inhibition (ZOI; diameter in mm) ± standard deviation (SD) at various concentrations			
		ZnO-NPs concentration (mg/mL)			Azithromycin (control)
		50 mg/mL	100 mg/mL	200 mg/mL	
Z20	*S. aureus*	27 ± 1.25	31 ± 1.75	32 ± 1.25	28 ± 0.25
	E. coli	22 ± 1.05	26 ± 0.25	27 ± 1.25	23 ± 0.25
Z30	*S. aureus*	29 ± 2.00	26 ± 1.75	34 ± 1.50	28 ± 0.50
	E. coli	22 ± 0.25	23 ± 0.25	25 ± 2.25	23 ± 0.25
Z40	*S. aureus*	13 ± 0.50	15 ± 0.25	17 ± 0.00	28 ± 0.25
	E. coli	12 ± 0.25	15 ± 0.50	16 ± 0.75	23 ± 0.50

the bacterial surface facilitated by surface potential, distortion of cell morphology, NPs penetration into cells, membrane damage due to structural and functional interruption, and leakage of cellular components, thus functionality loss [9, 47, 48]; (ii) Zn^{2+} release from ZnO-NPs which, up on penetration into the cell, can inhibit several bacterial activities including transports, metabolisms, and enzyme functions, leading to cell death; (iii) ZnO activity as a result of the formation of reactive oxygen species (ROS) which leads to oxidative stress and subsequent cell damage [49]. An illustration of the proposed mechanism is given in Figure 7.

3.3. Biocompatibility of ZnO-NPs with Human Erythrocytes. Biocompatibility of ZnO-NPs was assessed using *in vitro* hemolysis assay at different concentrations 3.12–200 μg/mL, against RBCs and in reference to NS and DW as negative and positive controls [21], respectively. Hemolysis is generally based on measuring hemoglobin released from RBC after sample-induced cell lysis. Figure 8 illustrates the averaged data obtained from the two experiments. As can be seen, the toxicity of ZnO-NPs at the evaluated highest concentration (200 μg/mL) was 17.4%, which agreed with the previous reports [11, 50]. The hemolysis effect at 3.12 and 6.25 μg/mL were around 4.6 and 7.5%, increased to 16.8% for 25 μg/mL

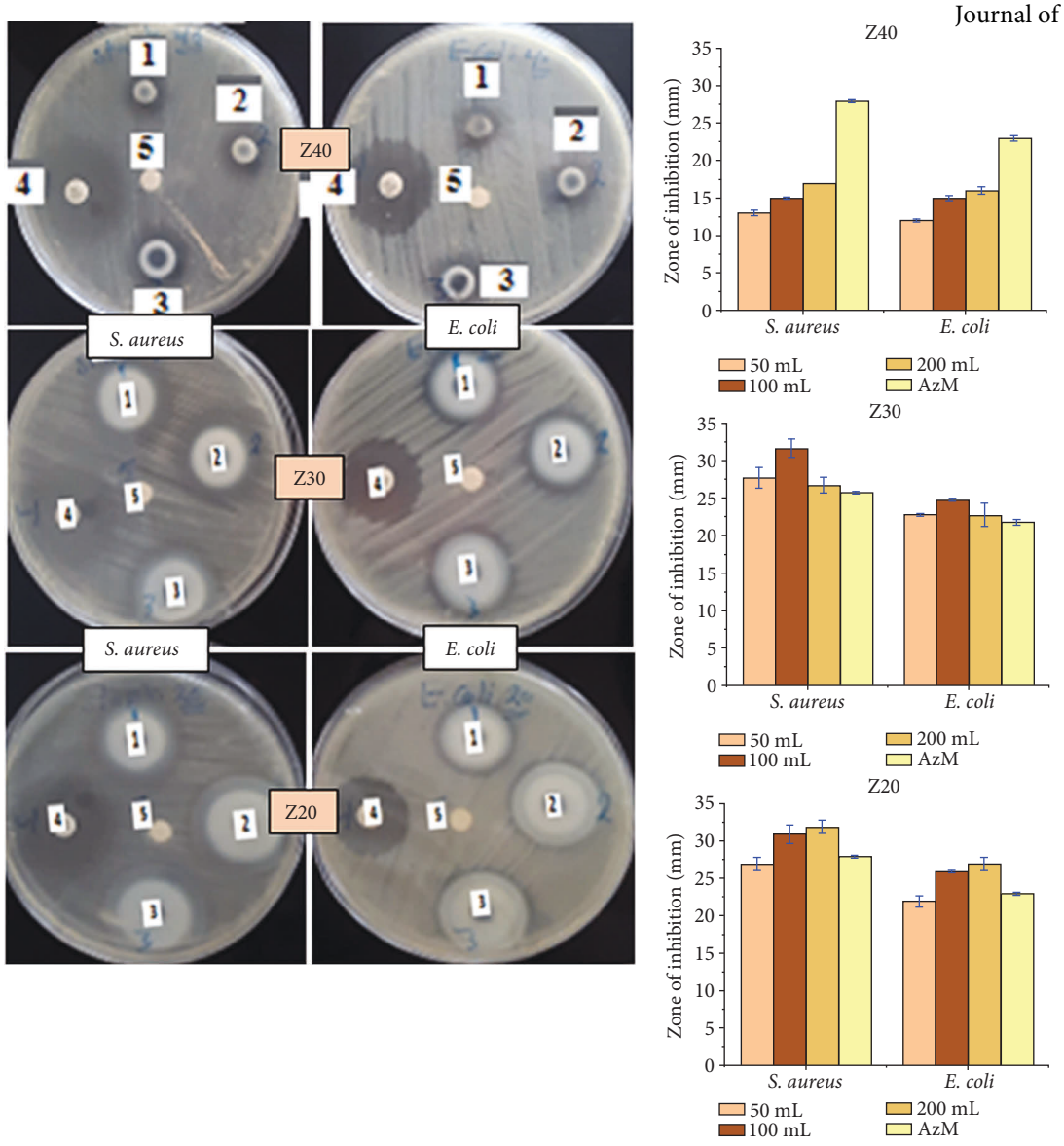

(a) (b)

Figure 6: (a) Selected plate images of antibacterial activity tests of ZnO-NPs prepared using 20, 30, and 40 mL PPE (from the bottom to the top: Z20, Z30, and Z40) against *S. aureus* (left images) and *E. coli* (right images). Disks: (1) ZnO-NPs 50 mg/mL per disc; (2) ZnO-NPs 100 mg/mL per disc; (3) ZnO-NPs 200 mg/mL per disc; (4) Azithromycin antibiotics (positive control); (5) distilled water (negative control). (b) Histogram illustration for the corresponding zone of inhibition data; bars represent the standard error of the mean ($n = 2$).

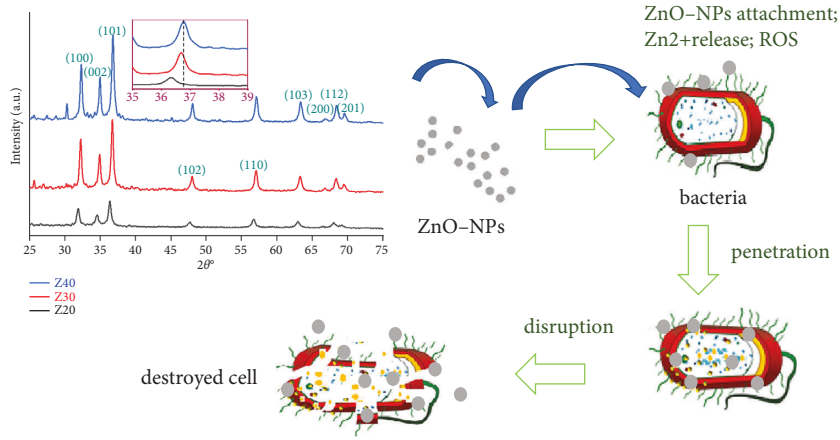

Figure 7: The proposed antibacterial mechanism of ZnO-NPs.

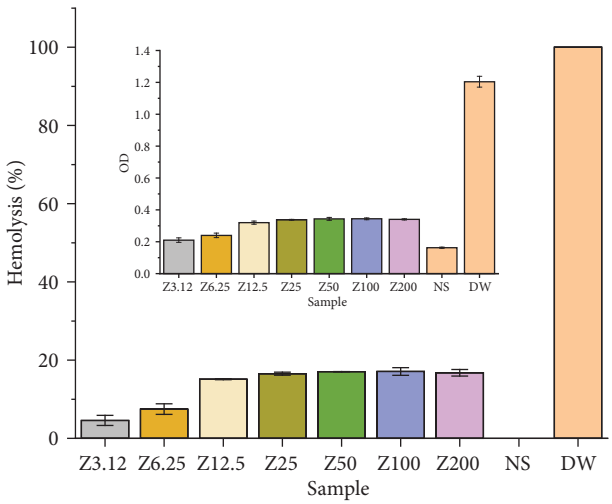

Figure 8: Hemolysis of erythrocytes caused by ZnO-NPs at different concentrations (3.12–200 μg/mL), normal saline (NS, negative control), and distilled water (DW, positive control). Insert is an illustration of samples absorption (OD) including controls.

above which no significant differences could be observed up to 200 μg/mL. Basically, substances with hemolysis <2% is standardized as nonhemolytic, 2–5% slightly hemolytic while >5% hemolytic [21]. The obtained values at low concentrations revealed low toxicity and are in agreement with the literature [50] stated that ZnO-NPs concentration lower than 5% is nontoxic, being slightly hemolytic under 5–40 μg/mL while hemolytic at > 40 μg/mL. Muhammad et at. [11], have reported a 21.8% hemolytic for ZnO-NPs at a concentration of 200 μg/mL, however researchers have detected no hemolysis at concentrations below 5 μg/mL. Meanwhile, the hemolytic effect of ZnO-NPs has been reported to be concentration-dependent [11, 50], other factors including test conditions (medium, cells, and positive and negative controls), parameters (sample concentration and incubation time), and the substance nature (biogenic source, particle shape, and size) have to be analyzed as well to elucidate slight differences among studies [51].

4. Conclusion

In this study, ZnO-NPs were biosynthesized using *pomegranate peel* aqueous extract. The resultant NPs, obtained from various extract concentrations (20, 30, and 40 mL), were characterized for their structural, optical, and morphological properties using FTIR, SEM, XRD, and UV-Vis. The method resulted in a hexagonal crystallite, with averaged diameters of 18.53, 29.88, and 30.34 nm and optical bandgaps of 2.87, 2.80 and 1.92 eV, respectively. The antibacterial activity of this as-obtained ZnO-NPs at concentrations of 50, 100, and 200 mg/mL, examined on *S. aureus* and *E. coli* and compared with AzM standard drug, revealed comparable activity to that of AzM, higher when particle size is low, and more efficient against Gram-positive (*S. aureus*) bacteria than Gram-negative (*E. coli*) and at higher ZnO-NPs concentration. Hence, it could be concluded that *pomegranate peel* extract is a good candidate for biosynthesis of ZnO-NPs and the utilized green method is effective in the production of ZnO-NPs with a tailorable particle size and morphology.

Data Availability

The data used to support the findings of this study are included within the article.

Conflicts of Interest

The authors declare that they have no conflicts of interest.

Acknowledgments

The authors are grateful to the Deanship of Scientific Research, King Saud University, for the support through the Vice Deanship of Scientific Research Chairs, Engineer Abdullah Bugshan research chair for Dental and Oral Rehabilitation. The authors are thankful to Dr. Abdullah Al-Jarfi and Dr Morad G. S. Saleh Laps for the help with biological experiments.

References

[1] M. Naseer, U. Aslam, B. Khalid, and B. Chen, "Green route to synthesize zinc oxide nanoparticles using leaf extracts of cassia fistula and melia azadarach and their antibacterial potential," *Scientific Reports*, vol. 10, pp. 1–10, 2020.

[2] H. R. Rajabi, F. Sajadiasl, H. Karimi, and Z. M. Alvand, "Green synthesis of zinc sulfide nanophotocatalysts using aqueous extract of Ficus Johannis plant for efficient photodegradation of some pollutants," *Journal of Materials Research and Technology*, vol. 9, pp. 15638–15647, 2020.

[3] R. Dobrucka and J. Długaszewska, "Biosynthesis and antibacterial activity of ZnO nanoparticles using Trifolium pratense flower extract," *Saudi Journal of Biological Sciences*, vol. 23, no. 4, pp. 517–523, 2016.

[4] P. Ramesh, A. Rajendran, and M. Meenakshisundaram, "Green syntheis of zinc oxide nanoparticles using flower extract cassia auriculata," *Journal of Nanoscience and Nanotechnology*, vol. 2, pp. 41–45, 2014.

[5] M. M. Khan, M. H. Harunsani, A. L. Tan, M. Hojamberdiev, Y. A. Poi, and N. Ahmad, "Antibacterial studies of ZnO and Cu-doped ZnO nanoparticles synthesized using aqueous leaf extract of Stachytarpheta jamaicensis," *BioNanoScience*, vol. 10, no. 4, pp. 1037–1048, 2020.

[6] R. Yuvakkumar, J. Suresh, and S. I. Hong, *Green Synthesis of Zinc Oxide Nanoparticles, Advanced Materials Research*, Trans Tech Publisher, Stafa-Zurich, Switzerland, 2014.

[7] S. Gunalan, R. Sivaraj, and V. Rajendran, "Green synthesized ZnO nanoparticles against bacterial and fungal pathogens," *Progress in Natural Science: Materials International*, vol. 22, no. 6, pp. 693–700, 2012.

[8] J. Xu, Y. Huang, S. Zhu, N. Abbes, X. Jing, and L. Zhang, "A review of the green synthesis of ZnO nanoparticles using plant extracts and their prospects for application in antibacterial textiles," *Journal of Engineered Fibers and Fabrics*, vol. 16, Article ID 155892502110462, 2021.

[9] M. G. Demissie, F. K. Sabir, G. D. Edossa, and B. A. Gonfa, "Synthesis of zinc oxide nanoparticles using leaf extract of lippia adoensis (koseret) and evaluation of its antibacterial activity," *Journal of Chemistry*, vol. 2020, Article ID 7459042, 9 pages, 2020.

[10] A. Alnehia, A. Al-Hammadi, A. Al-Sharabi, and H. Alnahari, "Optical, structural and morphological properties of ZnO and Fe+ 3 doped ZnO-NPs prepared by Foeniculum vulgare extract as capping agent for optoelectronic applications," *Inorganic Chemistry Communications*, vol. 143, Article ID 109699, 2022.

[11] W. Muhammad, N. Ullah, M. Haroon, and B. H. Abbasi, "Optical, morphological and biological analysis of zinc oxide nanoparticles (ZnO NPs) using Papaver somniferum L," *RSC Advances*, vol. 9, no. 51, pp. 29541–29548, 2019.

[12] W. Ahmad and D. Kalra, "Green synthesis, characterization and anti microbial activities of ZnO nanoparticles using Euphorbia hirta leaf extract," *Journal of King Saud University Science*, vol. 32, no. 4, pp. 2358–2364, 2020.

[13] X. Chen, H. Zhang, J. Li, and L. Chen, "Analysis of chemical compounds of pomegranate peel polyphenols and their antibacterial action against Ralstonia solanacearum," *South African Journal of Botany*, vol. 140, pp. 4–10, 2021.

[14] N. Seeram, R. Lee, M. Hardy, and D. Heber, "Rapid large scale purification of ellagitannins from pomegranate husk, a by-product of the commercial juice industryfication of ellagitannins from pomegranate husk, a by-product of the commercial juice industry," *Separation and Purification Technologyfication Technology*, vol. 41, no. 1, pp. 49–55, 2005.

[15] N. S. Al-zoreky, "Antimicrobial activity of pomegranate (Punica granatum L.) fruit peels," *International Journal of Food Microbiology*, vol. 134, no. 3, pp. 244–248, 2009.

[16] S. H. Mun, R. Kong, Y. S. Seo et al., "Subinhibitory Concentrations of Punicalagin reduces expression of virulence-related exoproteins by *Staphylococcus aureus*," *FEMS Microbiology Letters*, vol. 363, no. 22, 2016.

[17] E. C. Rosas-Burgos, A. Burgos-Hernandez, L. Noguera-Artiaga et al., "Antimicrobial activity of pomegranate peel extracts as affected by cultivar," *Journal of the Science of Food and Agriculture*, vol. 97, no. 3, pp. 802–810, 2017.

[18] F. Mukhtar, T. Munawar, M. S. Nadeem, M. N. U. Rehman, M. Riaz, and F. Iqbal, "Dual S-scheme heterojunction ZnO–V2O5–WO3 nanocomposite with enhanced photocatalytic and antimicrobial activity," *Materials Chemistry and Physics*, vol. 263, Article ID 124372, 2021.

[19] I. Al-Qadsy, W. S. Saeed, A.-B. Al-Odayni, L. Ahmed Saleh Al-Faqeeh, A. A. Alghamdi, and M. Farooqui, "Novel metformin-based schiff bases: synthesis, characterization, and antibacterial evaluation," *Materials*, vol. 13, no. 3, p. 514, 2020.

[20] M. M. S. Saif, R. M. Alodeni, A. A. Alghamdi, and A.-B. Al-Odayni, "Synthesis, spectroscopic characterization, thermal analysis and in vitro bioactivity studies of the N-(cinnamylidene) tryptophan Schiff base," *Journal of King Saud University Science*, vol. 34, no. 4, Article ID 101988, 2022.

[21] D. Guowei, K. Adriane, X. Chen, C. Jie, and L. Yinfeng, "PVP magnetic nanospheres: biocompatibility, in vitro and in vivo bleomycin release," *International Journal of Pharmaceutics*, vol. 328, no. 1, pp. 78–85, 2007.

[22] S. Saleem, M. H. Jameel, N. Akhtar et al., "Modification in structural, optical, morphological, and electrical properties of zinc oxide (ZnO) nanoparticles (NPs) by metal (Ni, Co) dopants for electronic device applications," *Arabian Journal of Chemistry*, vol. 15, no. 1, Article ID 103518, 2022.

[23] A. A. Alghamdi, A.-B. Al-Odayni, W. S. Saeed et al., "Adsorption of azo dye methyl orange from aqueous solutions using alkali-activated polypyrrole-based graphene oxide," *Molecules*, vol. 24, no. 20, p. 3685, 2019.

[24] H. Yang, Y.-y. Ren, T. Wang, and C. Wang, "Preparation and antibacterial activities of Ag/Ag+/Ag3+ nanoparticle composites made by pomegranate (Punica granatum) rind extract," *Results in Physics*, vol. 6, pp. 299–304, 2016.

[25] W. M. Husain, J. K. Araak, and O. M. Ibrahim, "Green Synthesis of zinc oxide Nanoparticles from (punica granatum L) pomegranate Aqueous peel Extract," *The Iraqi Journal of Veterinary Medicine*, vol. 43, no. 2, pp. 6–14, 2019.

[26] R. Amooaghaie, M. R. Saeri, and M. Azizi, "Synthesis, characterization and biocompatibility of silver nanoparticles synthesized from Nigella sativa leaf extract in comparison with chemical silver nanoparticles," *Ecotoxicology and Environmental Safety*, vol. 120, pp. 400–408, 2015.

[27] A. Y. Ghidan, T. M. Al-Antary, N. M. Salem, and A. M. Awwad, "Facile green synthetic route to the zinc oxide (ZnONPs) nanoparticles: effect on green peach aphid and antibacterial activity," *Journal of Agricultural Science*, vol. 9, no. 2, pp. 131–138, 2017.

[28] U. L. Ifeanyichukwu, O. E. Fayemi, and C. N. Ateba, "Green synthesis of zinc oxide nanoparticles from pomegranate (Punica granatum) extracts and characterization of their antibacterial activity," *Molecules*, vol. 25, no. 19, p. 4521, 2020.

[29] S. Azizi, R. Mohamad, A. Bahadoran et al., "Effect of annealing temperature on antimicrobial and structural properties of bio-synthesized zinc oxide nanoparticles using flower extract of Anchusa italica," *Journal of Photochemistry and Photobiology B: Biology*, vol. 161, pp. 441–449, 2016.

[30] A. Al-Osta, A. Alnehia, A. A. Qaid, H. T. Al-Ahsab, and A. Al-Sharabi, "Structural, morphological and optical properties of Cr doped ZnS nanoparticles prepared without any capping agent," *Optik*, vol. 214, Article ID 164831, 2020.

[31] M. M. Khan, N. Ahmad, M. H. Harunsani et al., *Antibacterial Studies of ZnO and Cu-Doped ZnO Nanoparticles Synthesized Using Aqueous Leaf Extract of Stachytarpheta Jamaicensis*, Bio Nano Science, San Diego, CA, USA, 2020.

[32] O. Sahin and S. Horoz, "Synthesis of Ni:ZnS quantum dots and investigation of their properties," *Journal of Materials Science: Materials in Electronics*, vol. 29, no. 19, pp. 16775–16781, 2018.

[33] K. C. Kumar, N. M. Rao, S. Kaleemulla, and G. V. Rao, "Structural, optical and magnetic properties of Sn doped ZnS nano powders prepared by solid state reaction," *Physica B: Condensed Matter*, vol. 522, pp. 75–80, 2017.

[34] A. Azmand and H. Kafashan, "Physical and electrochemical properties of electrodeposited undoped and Se-doped ZnS thin films," *Ceramics International*, vol. 44, no. 14, pp. 17124–17137, 2018.

[35] M. Rafique, M. Sohaib, R. Tahir et al., "Novel, facile and first time synthesis of zinc oxide nanoparticles using leaves extract of Citrus reticulata for photocatalytic and antibacterial activity," *Optik*, vol. 243, Article ID 167495, 2021.

[36] M. S. Nadeem, T. Munawar, F. Mukhtar et al., "Hydrothermally derived co, Ni co-doped ZnO nanorods; structural, optical, and morphological study," *Optical Materials*, vol. 111, Article ID 110606, 2021.

[37] T. Munawar, S. Yasmeen, F. Mukhtar et al., "$Zn_{0.9}Ce_{0.05}MO$ (M = Er, Y, V) nanocrystals: structural and energy bandgap engineering of ZnO for enhancing photocatalytic and antibacterial activity," *Ceramics International*, vol. 46, no. 10, pp. 14369–14383, 2020.

[38] M. D. Jayappa, C. K. Ramaiah, M. A. P. Kumar et al., "Green synthesis of zinc oxide nanoparticles from the leaf, stem and in vitro grown callus of Mussaenda frondosa L.: characterization and their applications," *Applied Nanoscience*, vol. 10, no. 8, pp. 3057–3074, 2020.

[39] C. Vidya, S. Hiremath, M. Chandraprabha et al., "Green synthesis of ZnO nanoparticles by Calotropis gigantea," *International Journal of Current Engineering and Technology*, vol. 1, pp. 118–120, 2013.

[40] M. M. Ba-Abbad, M. S. Takriff, A. Benamor, E. Mahmoudi, and A. W. Mohammad, "Arabic gum as green agent for ZnO nanoparticles synthesis: properties, mechanism and antibacterial activity," *Journal of Materials Science: Materials in Electronics*, vol. 28, no. 16, pp. 12100–12107, 2017.

[41] A. Abdulwahab, E. A. Al-Mahdi, A. Al-Osta, and A. Qaid, "Structural, optical and electrical properties of CuSCN nanopowders doped with Li for optoelectronic applications," *Chinese Journal of Physics*, vol. 73, pp. 479–492, 2021.

[42] B. Poornaprakash, U. Chalapathi, Y. Suh, S. P. Vattikuti, M. S. P. Reddy, and S.-H. Park, "Terbium-doped ZnS quantum dots: structural, morphological, optical, photoluminescence, and photocatalytic properties," *Ceramics International*, vol. 44, no. 10, pp. 11724–11729, 2018.

[43] U. A. Minha Nasser, B. Khalid, and B. Chen, "green route to synthesize zinc oxide nanoparticles using leaf extracts of cassia fistula and melia azadarach and their antibacterial potential," *Scientific Reports*, vol. 10, 2020.

[44] A. Rahman, M. H. Harunsani, A. L. Tan, N. Ahmad, B. K. Min, and M. M. Khan, "Influence of Mg and Cu dual-doping on phytogenic synthesized ZnO for light induced antibacterial and radical scavenging activities," *Materials Science in Semiconductor Processing*, vol. 128, Article ID 105761, 2021.

[45] S. M. Sathish kumar Mani, V. Muthusamy, and R. Thangaraj, "Antimicrobial activity and photocatalytic degradation properties of zinc sulfide nanoparticles synthesized by using plant extracts," *J Nanostruct*, vol. 8, pp. 107–118, 2018.

[46] B. Ahmed, B. Solanki, A. Zaidi, M. S. Khan, and J. Musarrat, "Bacterial toxicity of biomimetic green zinc oxide nanoantibiotic: insights into ZnONP uptake and nanocolloid–bacteria interface," *Toxicology research*, vol. 8, no. 2, pp. 246–261, 2019.

[47] B. Ahmed, F. Ameen, A. Rizvi et al., "Destruction of cell topography, morphology, membrane, inhibition of respiration, biofilm formation, and bioactive molecule production by nanoparticles of Ag, ZnO, CuO, TiO2, and Al2O3 toward beneficial soil bacteria," *ACS Omega*, vol. 5, no. 14, pp. 7861–7876, 2020.

[48] S. Soren, S. Kumar, S. Mishra, P. K. Jena, S. K. Verma, and P. Parhi, "Evaluation of antibacterial and antioxidant potential of the zinc oxide nanoparticles synthesized by aqueous and polyol method," *Microbial Pathogenesis*, vol. 119, pp. 145–151, 2018.

[49] H. Agarwal, S. Menon, S. Venkat Kumar, and S. Rajeshkumar, "Mechanistic study on antibacterial action of zinc oxide nanoparticles synthesized using green route," *Chemico-Biological Interactions*, vol. 286, pp. 60–70, 2018.

[50] A. T. Khalil, M. Ovais, I. Ullah et al., "Sageretia thea (Osbeck.) mediated synthesis of zinc oxide nanoparticles and its biological applications," *Nanomedicine*, vol. 12, no. 15, pp. 1767–1789, 2017.

[51] E. Preedia Babu, A. Subastri, A. Suyavaran et al., "Size dependent uptake and hemolytic effect of zinc oxide nanoparticles on erythrocytes and biomedical potential of ZnO-ferulic acid conjugates," *Scientific Reports*, vol. 7, pp. 4203–4212, 2017.